This version is available at https://strathprints.strath.ac.uk/61816/

Research Paper

Electrospun collagen-based nanofibres: A sustainable material for improved antibiotic utilisation in tissue engineering applications

Ivan J. Hall Barrientos[a,b], Eleonora Paladino[b,c,d], Peter Szabó[e], Sarah Brozio[b], Peter J. Hall[f], Charles I. Oseghale[f], Melissa K. Passarelli[d], Susan J. Moug[g], Richard A. Black[a], Clive G. Wilson[b], Romana Zelkó[e,**], Dimitrios A. Lamprou[b,h,*]

[a] Biomedical Engineering, University of Strathclyde, Glasgow, United Kingdom
[b] Strathclyde Institute of Pharmacy and Biomedical Sciences (SIPBS), University of Strathclyde, 161 Cathedral Street, Glasgow, G4 0RE, United Kingdom
[c] EPSRC Centre for Innovative Manufacturing in Continuous Manufacturing and Crystallisation (CMAC), University of Strathclyde, Technology and Innovation Centre, 99 George Street, G1 1RD Glasgow, United Kingdom
[d] National Physical Laboratory (NPL), Hampton Road, Teddington, Middlesex, TW11 0LW, United Kingdom
[e] University Pharmacy Department of Pharmacy Administration, H-1092 Budapest, Hőgyes Endre u. 7–9, Hungary
[f] Kroto Research Institute, University of Sheffield, Sheffield, S3 7HQ, United Kingdom
[g] National Health Service (NHS), Royal Alexandra Hospital, Paisley, PA2 9PN, United Kingdom
[h] Medway School of Pharmacy, University of Kent, Medway Campus, Anson Building, Central Avenue, Chatham Maritime, Chatham, Kent, ME4 4TB, United Kingdom

ARTICLE INFO

ABSTRACT

For the creation of scaffolds in tissue engineering applications, it is essential to control the physical morphology of fibres and to choose compositions which do not disturb normal physiological function. *Collagen*, the most abundant protein in the human body, is a well-established biopolymer used in electrospinning compositions. It shows high *in-vivo* stability and is able to maintain a high biomechanical strength over time. In this study, the effects of collagen type I in polylactic acid-drug electrospun scaffolds for tissue engineering applications are examined. The samples produced were subsequently characterised using a range of techniques. Scanning electron microscopy analysis shows that the fibre morphologies varied across PLA-drug and PLA-collagen-drug samples – the addition of collagen caused a decrease in average fibre diameter by nearly half, and produced nanofibres. Atomic force microscopy imaging revealed collagen-banding patterns which show the successful integration of collagen with PLA. Solid-state characterisation suggested a chemical interaction between PLA and drug compounds, irgasan and levofloxacin, and the collagen increased the amorphous regions within the samples. Surface energy analysis of drug powders showed a higher dispersive surface energy of levofloxacin compared with irgasan, and contact angle goniometry showed an increase in hydrophobicity in PLA-collagen-drug samples. The antibacterial studies showed a high efficacy of resistance against the growth of both *E. coli* and *S. Aureus*, except with PLA-collagen-LEVO which showed a regrowth of bacteria after 48 h. This can be attributed to the low drug release percentage incorporated into the nanofibre during the *in vitro* release study. However, the studies did show that collagen helped shift both drugs into sustained release behaviour. These ideal modifications to electrospun scaffolds may prove useful in further research regarding the acceptance of human tissue by inhibiting the potential for bacterial infection.

© 2017 The Authors. Published by Elsevier B.V. This is an open access article under the CC BY license (http://creativecommons.org/licenses/by/4.0/).

1. Introduction

Within the field of tissue engineering, there are a number of different applications that can be explored relating to the combination of synthetic and natural polymers, and integration with various active pharmaceutical ingredients. For example, surgical wound closure involves the bringing together of opposing surfaces using glues, staples and/or sutures. The re-joined tissues

* Corresponding author at: Medway School of Pharmacy, University of Kent, Medway Campus, Anson Building, Central Avenue, Chatham Maritime, Chatham, Kent, ME4 4TB, United Kingdom.
** Corresponding author.
E-mail addresses: zelko.romana@pharma.semmelweis-univ.hu (R. Zelkó), d.lamprou@kent.ac.uk (D.A. Lamprou).

then undergo a primary hyper-proliferative stage, characterised by clot formation and the recruitment of inflammatory cells (macrophages) into the wound (Koh and DiPietro, 2011). Secretion of local tissue mediators encourages cell migration and begins the process of scar formation (Hu et al., 2014). Wound contraction, a result of tissue remodelling, increases the tensile strength of skin across lesions and increases (or decreases) the risk of ruptures. During the healing stage, the tissue is open to infection itself and as a pathway into deeper tissue structures. Infection can result in significant complications (e.g. prolonged systemic antibiotic administration, re-operation for debridement) for the patient in the short and long-term. In supporting healing, the purpose of an added matrix task may be to provide tensile strength, to encourage controlled epithelialisation and new vascular growth and to decrease the formation of bacterial biofilms. The fabrication of scaffolds for wound repair has become important, especially the formation of tissue-specific scaffolds (van Winterswijk and Nout, 2007).

For the creation of scaffolds it is essential to mimic the chemical composition, the physical morphology, and the biological functions of the human body (Jiang et al., 2013). Scaffolds can be created using synthetic polymers (e.g. polycaprolactone) or natural polymers (e.g. chitosan), or a combination of both − the addition of natural polymers can be highly advantageous as these may avoid the stimulation of chronic inflammation, immunological reactions and toxicity (Mano et al., 2007). An example of a natural polymer is *collagen*, which is the most abundant protein in the human body, a key element of the extracellular matrix (ECM), and imparts structural integrity and tensile strength to tissues (Sell et al., 2009). Using collagen in scaffolds has been previously shown to show a high in vivo stability and is able to maintain a high biomechanical strength over time (Tillman et al., 2009).

One method that is commonly used to fabricate scaffolds for tissue engineering is *electrospinning*. The technique utilises electrostatic forces to stretch a dilute polymer solution as it solidifies (Del Valle et al., 2011). It is an ideal micro- and nanofibre fabrication technique for tissue engineering, as the fibres within the resulting scaffold closely mimic the size and structure of the native extracellular matrix (Tan et al., 2008) and the use of solvent and aqueous based systems are useful for the integration of biological compounds, such as collagen. Various practices of electrospinning collagen, including collagen-elastin blends (Buttafoco et al., 2006), collagen-polycaprolactone scaffolds for vascular tissue engineering (Venugopal et al., 2005), and fibrinogen fibres which allows native deposits of collagen during cell growth (McManus et al., 2006) have previously been studied. Despite these examples of electrospinning involving collagen, there is an apparent gap in the research concerning the integration of drugs in these electrospun scaffolds. The integration of drugs, such as antibiotics, with polymer-collagen blends may be critical in the future success of human tissue accepting the scaffolds; there are many clinical applications for scaffolds that require controlling growth of bacteria. For example, one of the requirements for controlling intra-abdominal infection is to maintain satisfactory levels of an antimicrobial drug during drug administration (Solomkin et al., 2010). In this regard, the sustained release of drugs is critical to the success of the device. Sustained release of drugs with electrospun materials have been previously studied, including polylactic acid with diclofenac sodium (an anti-inflammatory agent) (Toncheva et al., 2011), metronidazole-loaded polycaprolactone nanofibres (He et al., 2016), and polyvinylidene fluoride with enrofloxacin (antibiotic) (He et al., 2015). Given the range of success there has been with electrospinning polymer with drug, and polymer-collagen blends, the next area of research should be to determine whether we can alter any of the characteristics of scaffolds with the inclusion of collagen, whether it be mechanical, chemical or drug release changes.

The purpose of this study is to examine the physicochemical properties, bacterial response, drug loading and bio-functionalisation of electrospun scaffolds that have been prepared using Type I Collagen with a supporting synthetic polymer. The polymer chosen for this study is *Polylactic-acid* (PLA), a biodegradable and biocompatible polymer. It has been approved by the US Food & Drug Administration for safe clinical use as resorbable sutures (Kimura and Ogura, 2001). PLA has also been used clinically for foot fractures (PLA pins) (Athanasiou et al., 1996), temporary implants (Nair and Schug, 2004) and drug delivery carriers (Ramot et al., 2016). In this study, solutions were modified by the addition of type I collagen. The matrix was loaded and electrospun with two drugs, *triclosan* (an antibacterial agent used commonly in soaps, detergents and surgical cleaning agents) or *levofloxacin* (a broad-spectrum quinolone antibiotic used commonly in clinical practice to treat gastrointestinal infections). The electrospun fibres were then characterised through various methods: the morphology of the electrospun fibres was characterised by scanning electron microscope (SEM) and Atomic Force Microscope (AFM), solid state characterisation was performed by x-ray powder diffraction (XRPD) and differential scanning calorimetry (DSC), surface characterisation of the two drugs was investigated by surface energy analysis (SEA) and contact angle goniometry (CAG), and drug efficacy (e.g. *in vitro* release studies, antibacterial studies and time-of-flight secondary ion mass spectrometry (ToF-SIMS)). The results from this study should help to build a profile of data in order to aid future work with regards to tissue engineering research specific to the controlled release of drugs.

2. Materials & methods

2.1. Materials

Polylactic acid (PLA) with a mixed molecular weight was the chosen polymer for this study and was used as purchased from the suppliers (Sigma-Aldrich, *GF45989881*), and the collagen used was type I from calf skin (Sigma-Aldrich, *C9791*). Irgasan (5-Chloro-2-(2,4-dichlorophenoxy)phenol), Triclosan, >97%, (Sigma-Aldrich, *72779*) and levofloxacin ((*S*)-9-fluoro-2,3-dihydro-3-methyl-10-(4-methylpiperazin-1-yl)-7-oxo-7*H*-pyrido[*1,2,3-de*]-1,4-benzoxazine-6-carboxylic acid) >98%, (Sigma-Aldrich, *28266*) were obtained commercially. The solvents used for the electrospinning were also commercially purchased from Sigma-Aldrich, specifically chloroform (anhydrous, containing amylenes as stabilizers grade, >99%), *N,N*-dimethylformamide (DMF, anhydrous grade 99.8%) and 1,1,1,3,3,3-hexafluoro-2-propanol, (GC grade >99%).

2.2. Preparation of PLA solutions

Investigations of the polymer-drug solutions prepared showed that the optimum w/w concentration for electrospinning was 8%. This particular concentration was used as previous experimentation revealed that higher concentrations did not result in suitable fibre formation (suitable meaning regular fibre diameters and no signs of beading, data not shown). PLA (8% w/w), and a 9:1 (w/w) ratio of chloroform (CLF) to *N,N*-dimethylformamide (DMF). For the formulations containing collagen type I, both polymers were solubilised in hexafluoropropanol (HFP) with a total polymer (collagen + PLA) concentration of 8%. PLA was blended with collagen containing 1% collagen ($M_{PLA}/[M_{Collagen} + M_{PLA}] \times 100$) (Powell and Boyce, 2009). Collagen at a 1% concentration was used as higher concentrations, in the range 2% to 10% w/w, yielded unstable and inconsistent fibre formations.

The solutions were mixed through 30 min in the centrifuge, a further 30 min in a sonicator and a final 1 h with a magnetic stirrer, which resulted in a solution that appeared homogeneous and

composed of a single phase. The solution was left overnight, and a further 30 min of sonication was applied the following morning in order to confirm the uniformity of the solution. For the irgasan-loaded solutions, the same method was applied, at a concentration of 1% irgasan w/w. The concentration of the levofloxacin-loaded solutions was adjusted to 0.5% w/w to facilitate accurate measurement of the drug release profile. All the solutions remained clear after preparation. This process was based on the method used by Hall Barrientos et al. (2016) for solution preparation (Hall Barrientos et al., 2016).

2.3. Electrospinning

Various scaffolds were fabricated for each polymeric solution, using an in-house electrospinning apparatus which consisted of a syringe pump (Harvard Apparatus PHD 2000 infusion, US) and two 30 kV high-voltage power supplies (Alpha III series, Brandenburg, UK). The polymer solution was loaded into a 5 ml glass syringe and fed through tubing with a metal needle tip attached at the end. The needle was clamped into place, to allow for a high-voltage supply to run through it − this allowed for an electric field to be created between the needle and the target plate. The syringe was clamped to a pump, which determined the specific injection flow rate of the polymeric solutions. For each of the three solutions (e.g. unloaded, irgasan loaded, and levofloxacin loaded), 3 varying flow rates of 0.5, 1 and 1.5 ml h^{-1} were applied across varying voltages of 2 kV–5 kV (across the needles) and 10 kV–18 kV (Hall Barrientos et al., 2016). A 21 gauge needle, at a deposition distance of between 10 and 12 cm was used. The process was performed at ambient room temperature (approximately 21 °C) with a relative humidity of between 2 and 4% (electrospinning was not performed if the relative humidity was greater than 5%). The solution was electro-spun onto the target that was covered with aluminium foil, in order for the final material to be removed and used for further characterisation.

2.4. Scanning electron microscopy

A scanning electron microscope (SEM) was used to determine the morphology and individual fibre diameter of the electrospun PLA solutions (PLA, PLA-IRG, PLA-LEVO, PLA-Collagen, PLA-Collagen-IRG, and PLA-Collagen-LEVO). A Hitachi TM-1000 SEM was used to analyse various samples, in which the samples were mounted on an aluminium plate with conductive tape. Images of fibres were taken at various locations of each electrospun PLA scaffold in order to determine the overall uniformity of fibres (n = 5). Prior to imaging, the samples were sputter coated with gold for 30 s using a Leica EM ACE200 vacuum coater, repeated three times in order to increase the conductivity of the samples. The samples were imaged in secondary electron mode at 5 kV.

2.5. Mathematical analysis of fibre diameters

Statistical comparisons of samples were conducted using SPSS 20.0 software package (SPSS Inc., Chicago IL, USA). Descriptive statistics, analysis of variance, Scheffé post hoc test and Kolgomorov-Smirnov test were performed using 50 individual fibre diameters of each samples obtained from the morphological analysis.

2.6. Atomic force microscopy

Further morphological analysis was undertaken through atomic force microscopy (AFM). A Multimode 8 microscope (Bruker, USA), with Scanasyst-Air probes (Bruker, USA) was used in Peak Force Quantitative Nano Mechanics (QNM) mode (Lamprou et al., 2013).

The imaging of the fibres was performed under ambient conditions, with a silicon cantilever probe (Bruker). The tip radius of the probe and the spring constant were calculated to be in the regions of 0.964 nm (18° tip half angle) and 0.3947 N/m, respectively. The scan sizes ranged from 200 nm to 25 μm, at a scan rate of 0.977 Hz with 512-sample resolution. The Roughness Average (Ra) values were determined by entering surface scanning data, and digital levelling algorithm values were determined using Nanoscope Analysis software V1.40 (Bruker USA). AFM images were collected from two different samples and at random spot surface sampling.

2.7. Differential scanning calorimetry (DSC)

Differential scanning calorimetry (DSC) was carried out using a Mettler Toledo DSC822 in order to examine the thermal properties of the electrospun PLA scaffolds. First, the scaffolds were cut, weighed and placed in the DSC specific aluminium discs. The disc was then sealed using a press and subsequently placed in the DSC instrument. The parameters for DSC analysis were set (parameters are detailed below) via the computer software. The analysis was then run which took approximately 20 min. The method included heating from 25 °C to 220 °C at 10 °C steps, using standard 40 μl aluminium discs, and each sample consisted of 4 mg.

2.8. X-Ray powder diffraction (XRPD)

XRPD was performed in a Bruker D2 Phaser machine and measurements were taken under CuKα radiation (λ = 1.5406 Å), 40 kV and 30 mA as X-ray source with K_b (Ni) filter. Diffraction patterns were collected with 2θ ranging from 3° to 70°.

2.9. Contact angle goniometry (CAG)

To monitor changes in wettability of the scaffolds, sessile drop contact angle for distilled water was measured by contact angle goniometry, using a contact angle goniometer (Kruss G30, Germany) (Lamprou et al., 2010).

2.10. Surface energy analysis

The dispersive surface energy of the raw drug samples was determined by inverse gas chromatography using a SEA–IGC (Surface Measurement Systems). The samples were packed into 30 cm (3 mm inside diameter) silanised glass columns, plugged at either end by silanised glass wool. Various dispersive probes were used; undecane, decane, nonane, octane, heptane, and hexane were injected at a range of fractional surface coverage in order to determine the concentration free dispersive surface energy (Gamble et al., 2012).

2.11. ^{1}H NMR studies

NMR spectra were recorded on a Varian 600 MHz spectrometer at 298.2 ± 0.1 K with CDCl3:DMF (N,N-dimethylformamide), 95:5, V/V% as solvent, using tetramethylsilane (TMS) as the chemical shift reference compound. The sample volume was 600 μl. 1H NMR spectra were recorded with the pulse and acquire sequence (number of transients = 16, number of points = 16384, acquisition time = 851.968 ms, relaxation delay = 1.5 s).

2.12. In vitro drug release studies

The drug releases of the irgasan/levofloxacin loaded PLA-blend scaffolds were measured in order to determine the release profile for each drug. Buffer solutions consisting of phosphate buffer

solution (PBS, pH 7.4) was mixed with 1% sodium dodecyl sulphate (SDS, a surfactant was used due to the hydrophobic nature of irgasan). The UV absorbance of both drugs were measured (irgasan at 280 nm (Rafqah et al., 2006), and levofloxacin at 293 nm (Shahwal et al., 2013), respectively) at various time points (e.g. 15 min, 30 min, 1 h, 2 h, 4 h, 8 h, 24 h and then every day up to 192 h). For every measurement 3 ml of solution was taken from the vial (consisting of total 6 ml PBS) and replaced with fresh 3 ml buffer in order to satisfy the perfect-sink conditions. The samples were stored in a temperature room of 37 °C.

2.13. Antibacterial studies

The antibacterial efficacy of the drug loaded electrospun scaffolds were tested with *Escherichia coli* (*E. coli*) 8739 and *Staphylococcus aureus* (*S. aureus*) 29213, bacterial strains representative of gram-negative and gram-positive bacteria, respectively. For this study, a disc agar diffusion method was used. Luria-Bertani (LB) agar was prepared with the LB medium consisting of 5 g tryptone, 2.5 g yeast extract, 5 g NaCl and 475 ml of deionized water. The *E. coli* and *S. aureus* cultures were grown overnight in 5 ml of solution, with both bacteria inoculated from a single colony. 150 μl of the *E. coli* and *S. aureus* cultures were spread onto plates of LB agar. 6 plates received an E. *coli* inoculum, and the other 6 plates contained the *S. aureus* inoculum, before adding small pieces of scaffold onto each plate. Scaffolds containing no drug and no scaffold presence acted as controls. Each scaffold was placed in triplicate to ensure accurate results. The plates were left for incubation for 48 h, and subsequently examined at 24 h and 48 h. Diameters of zones in which there was no bacterial growth were measured, and these were compared across the various drugs and bacterial strains.

2.14. Time of flight secondary ion mass spectrometry (ToF-SIMS)

The analyses were carried out with a ToF-SIMS V instrument (ION-TOF GmbH, Münster, Germany) equipped with a Bismuth cluster Liquid Metal Ion Gun (LMIG). To overcome charge build-up on the isolative samples, a low-energy electron beam (21 eV) flood gun was employed and the sample surface potential was optimised for each analysis.

Spectrometry mode was applied to acquire reference spectra of Levofloxacin, Irgasan and PLA. Data was recorded in three replicates for both polarities and each acquisition was made from different areas of the samples used in this study, over a field of view of 100 μm × 100 μm. The 30 kV Bi_3^+ primary ion beam was optimised to deliver a final primary ion dose density (PIDD) of 8.0×10^{12} (primary ions/cm^2) for each spectrum.

High lateral resolution images of the four drug-loaded samples were collected over a surface area of 50 μm × 50 μm, with a resolution of 512 × 512 pixels (pixel width was circa 0.1 μm), in the negative secondary ion polarity, with a final PIDD equal to 8.0×10^{12} primary ions/cm^2. The images were then processed using SurfaceLab 6.7 software (ION-TOF, Münster, Germany). All the mass spectral information was recorded in the m/z range of 0–900 Da.

3. Results

3.1. Intermolecular interactions

Preliminary ^{1}H NMR study performed in liquid phase suggests the absence of any specific intermolecular interaction between PLA and LEVO. The ^{1}H NMR spectrum of polylactic revealed two well-defined peaks centered at 5.10 and 1.52 (ppm) with smaller peaks residing in the vicinity of the main signal (less than 2% in total peak
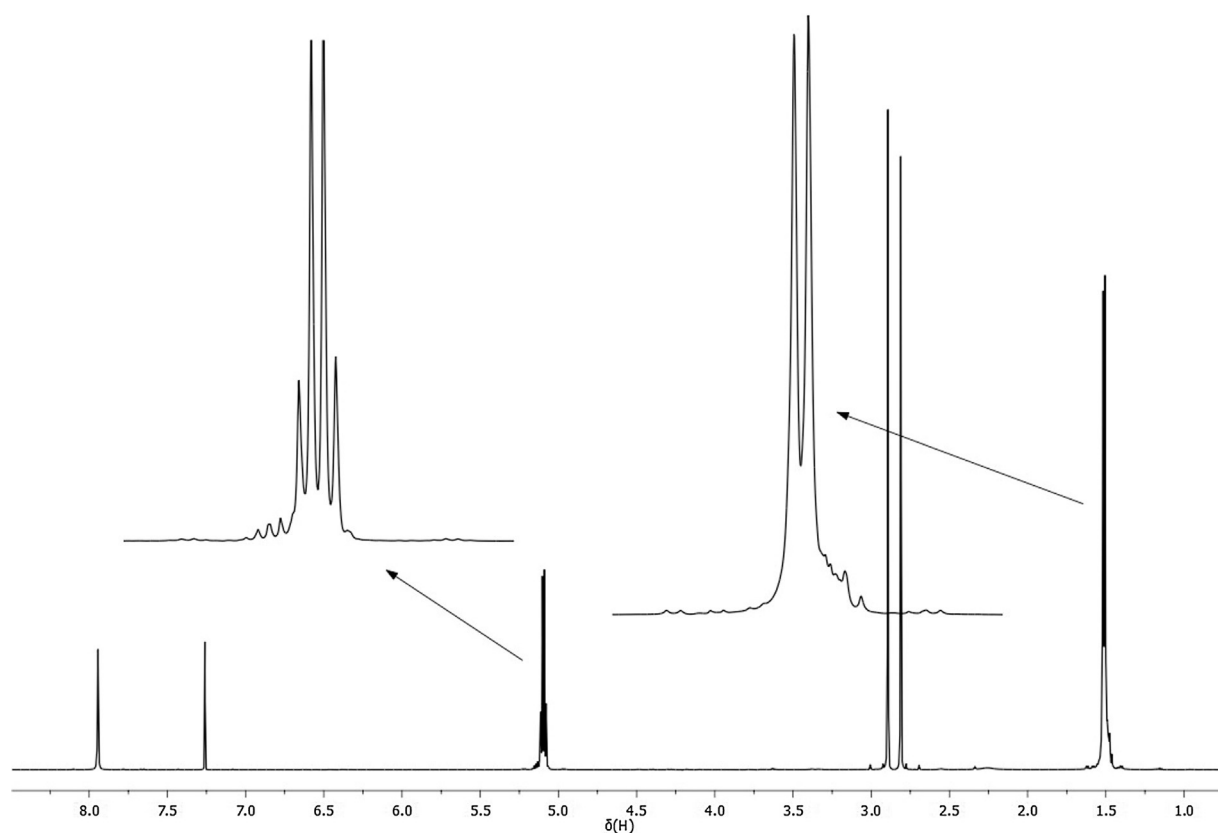

Fig. 1. The ^{1}H NMR spectrum of polylactic acid in CDCl3:DMF, 95:5, V/V%.

area based on Lorentz peak fitting) as depicted in Fig. 1. The relatively sharp (2–3 Hz half width) and uniform quartet and doublet signals of polylactic acid indicate a well-defined conformation throughout the polymer chain, and albeit the varying chain length the chemical environment of most monomer units is implied to be highly similar allowing for high mobility on account of the narrow peaks, i.e. high T2. The peaks at 7.26, 7.94, 2.89, and 2.81 are that of CHCl3, the formyl hydrogen of DMF, and the two methyl peaks of DMF, respectively. The ^{1}H NMR spectrum of polylactic acid doped with 0.1% levofloxacin showed no difference in the NMR parameters of the polymer; the peaks of levofloxacin were detected at the expected chemical shift ranges, however these signals appeared with too low SNR to be useful for further measurements. It can only be inferred from the NMR measurements that a possible presence of intermolecular interaction between polylactic acid and levofloxacin does not bring about detectable changes in the ^{1}H NMR spectra.

3.2. Fibre morphology

A one-way between-groups analysis of variance (ANOVA) indicated that there are significant differences ($p < 0.001$) between the investigated formulations. Applying Scheffé post-hoc comparison, significant differences were confirmed between samples except for PLA compared with PLA-IRG and PLA-Collagen compared with PLA-Collagen-IRG. The latter was also corroborated by the overlap between the obtained confidence intervals; whilst in case of the other samples the confidence intervals are separated from each other. Except for PLA-Collagen-LEVO, 99.7% of the measured fibre diameters fall between the range of mean ± 3 SD, and similarities of the mean and median values suggest that these samples are normally distributed (Fig. 2).

Fibre diameter histograms were assayed using Kolgomorov-Smirnov test ($p < 0.01$) of equality of distributions (Table 2), which indicated that there is no significant difference, when PLA compared with PLA-IRG; and PLA-Collagen compared with PLA-Collagen-IRG. On the other hand, distributions of PLA/PLA-IRG; PLA-Collagen/PLA-Collagen-IRG; PLA-LEVO; PLA-Collagen-LEVO were significantly different when compared with each other. It must be noted that PLA-Collagen-LEVO exhibited the highest coefficient of variation (72.7%), whilst PLA-LEVO had the lowest value (17.2%) (Table 1).

The SEM images (Fig. 3) demonstrated a range of morphologies across both polymer-drug and polymer-collagen-drug electrospun scaffolds. The PLA-drug scaffolds (Fig. 3a–c) showed consistent fibre diameter and the addition of IRG and LEVO caused very slight beading within the fibres.

The AFM images (Fig. 4) show the morphology of the fibres at a greater detail and resolution. PLA-drug scaffolds (Fig. 4a–b) show a slight variation of morphology across their surfaces; PLA fibres have a relatively smooth surface with what appears to be beading (possible solvent residue) on the surface, PLA-IRG fibres generally showed smooth morphology with no signs of active pharmaceutical ingredient (API) or solvent residue on the surface, whereas the PLA-LEVO fibres showed a rougher morphology which may have resulted from crystals of the drug at the surface – this observation was supported by the release profile (see: Results, Drug Efficacy). The surface morphology for the PLA-collagen-drug scaffolds
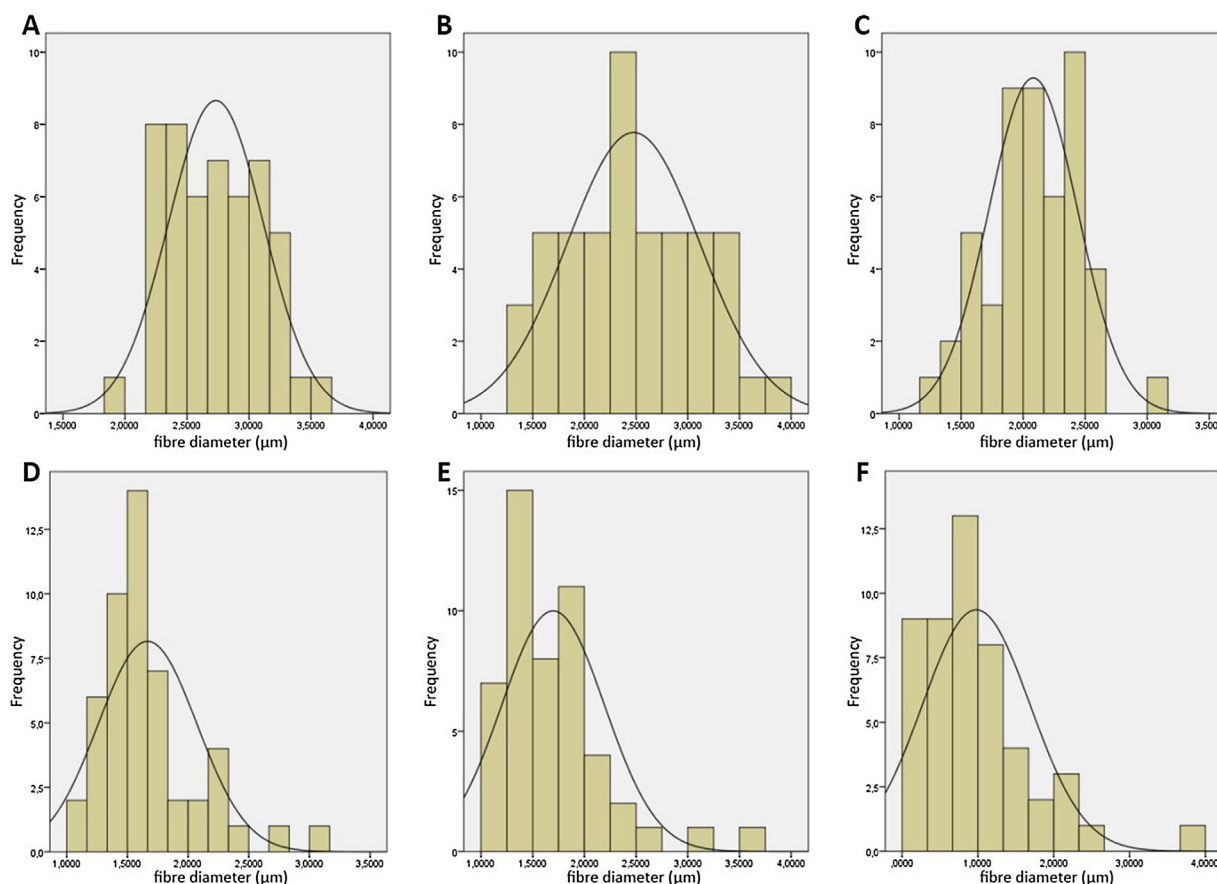

Fig. 2. Histograms of fibre diameters (a) PLA Unloaded, (b) PLA-IRG, (c) PLA-LEVO, (d) PLA-Collagen (e) PLA-Collagen-IRG, and (f) PLA-Collagen-LEVO.

Table 1
Descriptive statistics of the electrospun fibre diameters.

	N	Mean	Std. Deviation	Std. Error	95% Confidence Interval for Mean		Minimum	Maximum	Median	Coefficient of variation%
					Lower Bound	Upper Bound				
PLA	50	2.73	0.38	0.05	2.62	2.84	1.86	3.62	2.73	30.70
PLA-IRG	50	2.48	0.64	0.09	2.29	2.66	1.28	3.78	2.42	25.90
PLA-LEVO	50	2.08	0.36	0.05	1.98	2.18	1.32	3.08	2.08	17.20
PLA-Collagen	50	1.67	0.41	0.06	1.55	1.78	1.06	3.02	1.57	24.47
PLA-Collagen-IRG	50	1.70	0.50	0.07	1.56	1.84	1.01	3.63	1.64	29.42
PLA-Collagen-LEVO	50	0.98	0.71	0.10	0.78	1.18	0.12	3.67	0.92	72.67

Table 2
Multiple Comparisons.

(I) adat		Mean Difference (I-J)	Std. Error	Sig.	95% Confidence Interval	
					Lower Bound	Upper Bound
PLA	PLA-IRG	0.2575600	0.1034985	0.291	−0.089176	0.604296
	PLA-LEVO	0.6521600[*]	0.1034985	0.000	0.305424	0.998896
	PLA-COLLAGEN	1.0665800[*]	0.1034985	0.000	0.719844	1.413316
	PLA_COLLAGEN_IRG	1.0354800[*]	0.1034985	0.000	0.688744	1.382216
	PLA_COLLAGEN_LEVO	1.7551000[*]	0.1034985	0.000	1.408364	2.101836
PLA-IRG	PLA	−0.2575600	0.1034985	0.291	−0.604296	0.089176
	PLA-LEVO	0.3946000[*]	0.1034985	0.014	0.047864	0.741336
	PLA-COLLAGEN	0.8090200[*]	0.1034985	0.000	0.462284	1.155756
	PLA_COLLAGEN_IRG	0.7779200[*]	0.1034985	0.000	0.431184	1.124656
	PLA_COLLAGEN_LEVO	1.4975400[*]	0.1034985	0.000	1.150804	1.844276
PLA-LEVO	PLA	−0.6521600[*]	0.1034985	0.000	−0.998896	−0.305424
	PLA-IRG	−0.3946000[*]	0.1034985	0.014	−0.741336	−0.047864
	PLA-COLLAGEN	0.4144200[*]	0.1034985	0.008	0.067684	0.761156
	PLA_COLLAGEN_IRG	0.3833200[*]	0.1034985	0.019	0.036584	0.730056
	PLA_COLLAGEN_LEVO	1.1029400[*]	0.1034985	0.000	0.756204	1.449676
PLA-COLLAGEN	PLA	−1.0665800[*]	0.1034985	0.000	−1.413316	−0.719844
	PLA-IRG	−0.8090200[*]	0.1034985	0.000	−1.155756	−0.462284
	PLA-LEVO	−0.4144200[*]	0.1034985	0.008	−0.761156	−0.067684
	PLA_COLLAGEN_IRG	−0.0311000	0.1034985	1.000	−0.377836	0.315636
	PLA_COLLAGEN_LEVO	0.6885200[*]	0.1034985	0.000	0.341784	1.035256
PLA_COLLAGEN_IRG	PLA	−1.0354800[*]	0.1034985	0.000	−1.382216	−0.688744
	PLA-IRG	−0.7779200[*]	0.1034985	0.000	−1.124656	−0.431184
	PLA-LEVO	−0.3833200[*]	0.1034985	0.019	−0.730056	−0.036584
	PLA-COLLAGEN	0.0311000	0.1034985	1.000	−0.315636	0.377836
	PLA_COLLAGEN_LEVO	0.7196200[*]	0.1034985	0.000	0.372884	1.066356
PLA_COLLAGEN_LEVO	PLA	−1.7551000[*]	0.1034985	0.000	−2.101836	−1.408364
	PLA-IRG	−1.4975400[*]	0.1034985	0.000	−1.844276	−1.150804
	PLA-LEVO	−1.1029400[*]	0.1034985	0.000	−1.449676	−0.756204
	PLA-COLLAGEN	−0.6885200[*]	0.1034985	0.000	−1.035256	−0.341784
	PLA_COLLAGEN_IRG	−0.7196200[*]	0.1034985	0.000	−1.066356	−0.372884

[*] The mean difference is significant at the 0.05 level.

(Fig. 4d–f) showed the presence of collagen "wrapping" the polymeric fibres in a helical manner. This morphology was consistent throughout, which may highlight a helical coating of the collagen through the fabricated scaffolds. There appeared to be no presence of drug on the surface of these fibres.

3.3. Solid state characterisation

The graphs in Fig. 5 indicate the various DSC isotherms for PLA-drug fibres (Fig. 5a), and PLA-Collagen fibres (Fig. 5b). For most of the samples, the glass transition temperature (T_g) is observed around 60 °C, the crystallisation temperature (T_c), an exothermic peak, is observed around 90–115 °C and the melting point, an endothermic peak, is observed at ~145 °C. Overall the T_c for PLA-drug samples is lower than the PLA-collagen-drug samples. In the case of PLA-IRG (Fig. 5a), the T_g appears to be suppressed and a T_c was not measured at all.

XRPD data shown in Fig. 6 indicate that PLA fibres are semi-crystalline, indicated by broad region, followed by a sharp peak at ~17°. It can be observed in Fig. 6a that the addition of IRG causes an increase in the crystallinity of the polymer-drug sample, due to the sharp polymer peak at ~17°. There are no significant peaks arising within the PLA-IRG graph related to the IRG intensity. The PLA-collagen-IRG graph indicates that the sample is in an amorphous state, due to the very broad peak observed from ~5° to ~25°. The graphs relating to the PLA-LEVO sample (Fig. 6b) show two significant peaks at ~7° (relating levofloxacin) and ~17° (relating to PLA). Again, the addition of collagen to these samples resulted in a broad amorphous peak ranging from ~5° to ~25°.

3.4. Surface analysis

The dispersive surface energy of powder irgasan was measured at 37.32 mJ/m², and a BET specific surface area of 0.0103 m²/g.
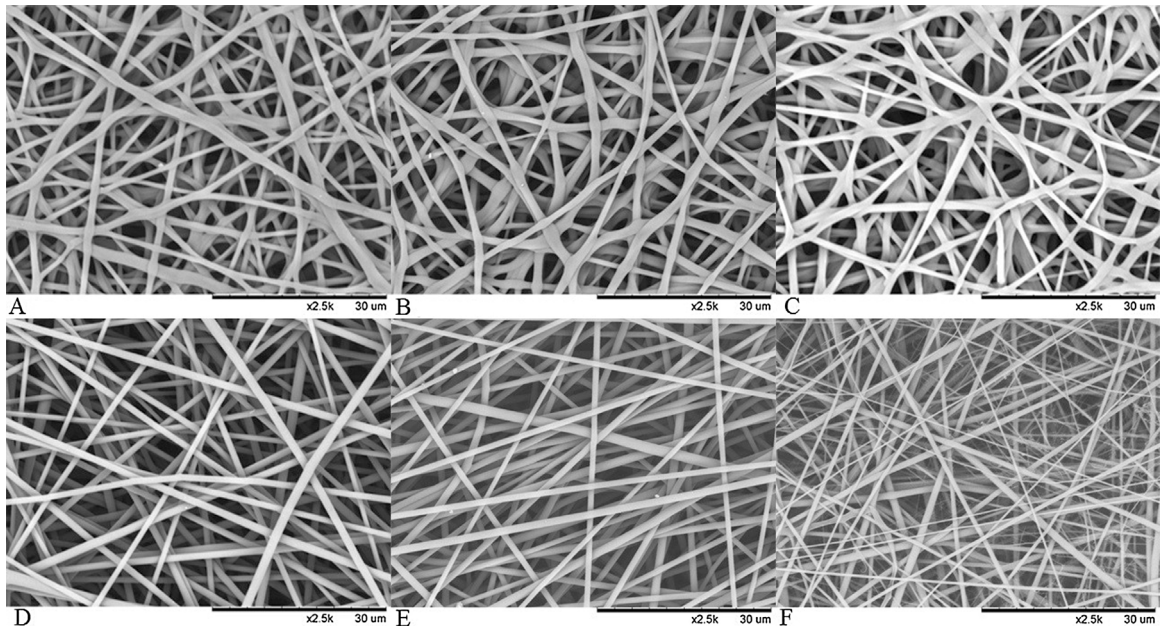
Fig. 3. SEM Images of: (a) PLA Unloaded, (b) PLA-IRG, (c) PLA-LEVO, (d) PLA-Collagen, (e) PLA-Collagen-IRG, and (f) PLA-Collagen-LEVO.
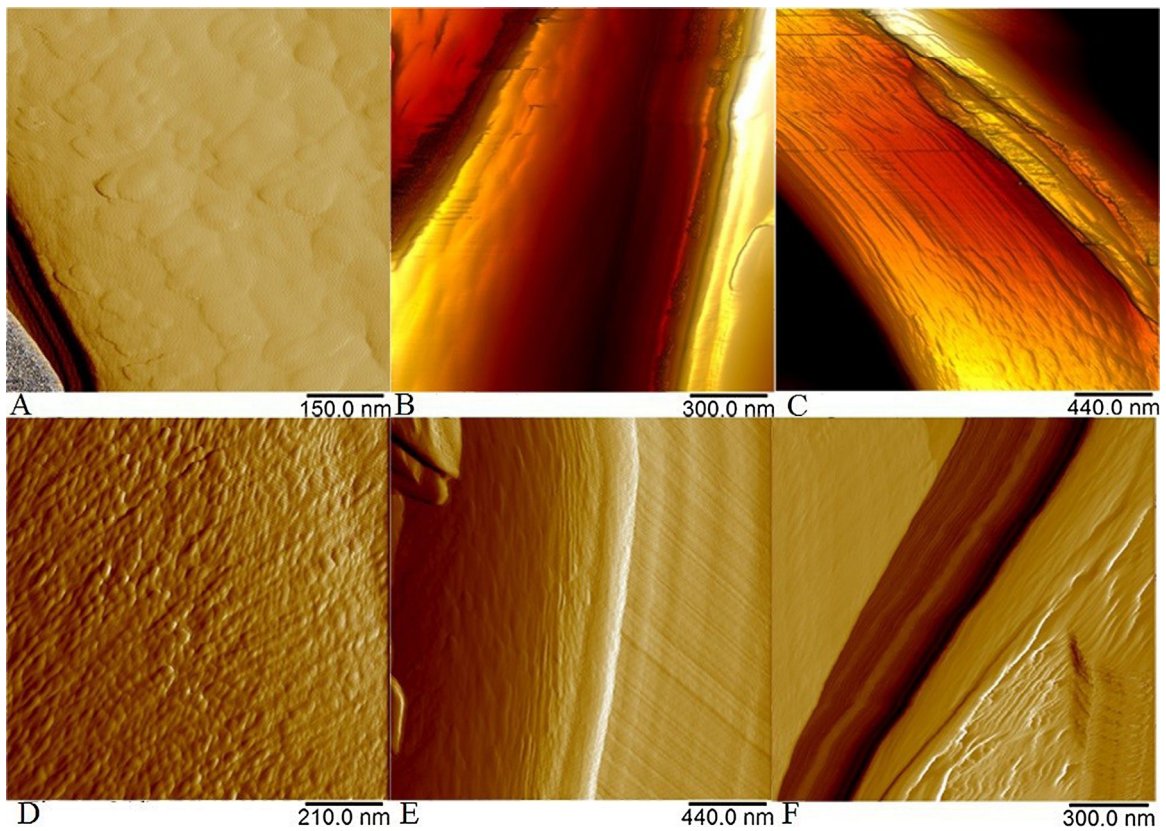

Fig. 4. AFM Images of (a) PLA Unloaded, (b) PLA-IRG, (c) PLA-LEVO, (d) PLA-Collagen (e) PLA-Collagen-IRG, and (f) PLA-Collagen-LEVO.

Levofloxacin had a higher dispersive surface energy of 47.34 mJ/m^2 and a BET specific surface area of 0.0481 m^2/g.

The contact angle measurements shown in Fig. 7 highlight the differences across PLA-drug and PLA-collagen-drug combinations; PLA-LEVO had a lower overall starting and finishing contact angle (108° ± 2.11 to 50° ± 2.35, respectively), compared with the PLA and PLA-IRG (120° ± 1.09 to 80° ± 1.22, respectively). The samples containing collagen had a greater starting contact angle (130° ± 3.42) and final contact angle reading (120° ± 4.12).

3.5. Drug efficacy and antibacterial studies

The cumulative drug release profiles are presented in Fig. 8; both PLA-IRG and PLA-collagen-IRG samples exhibited sustained
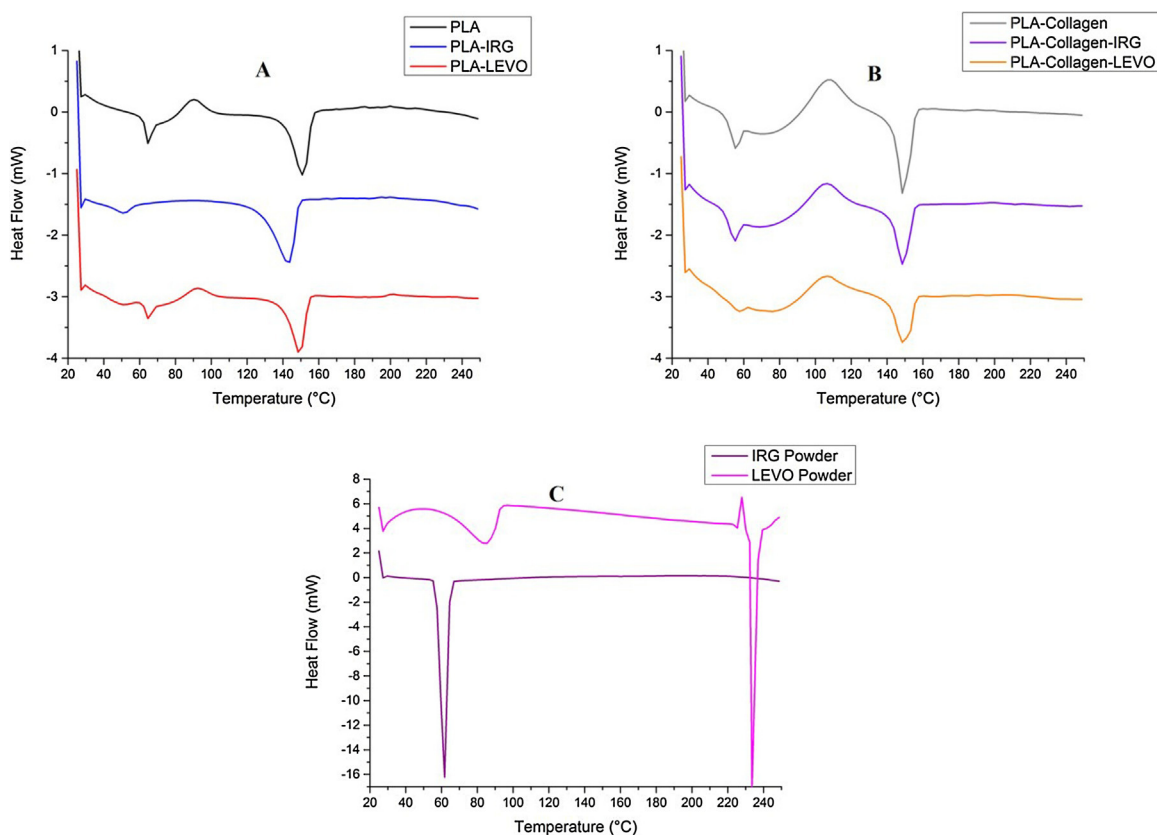
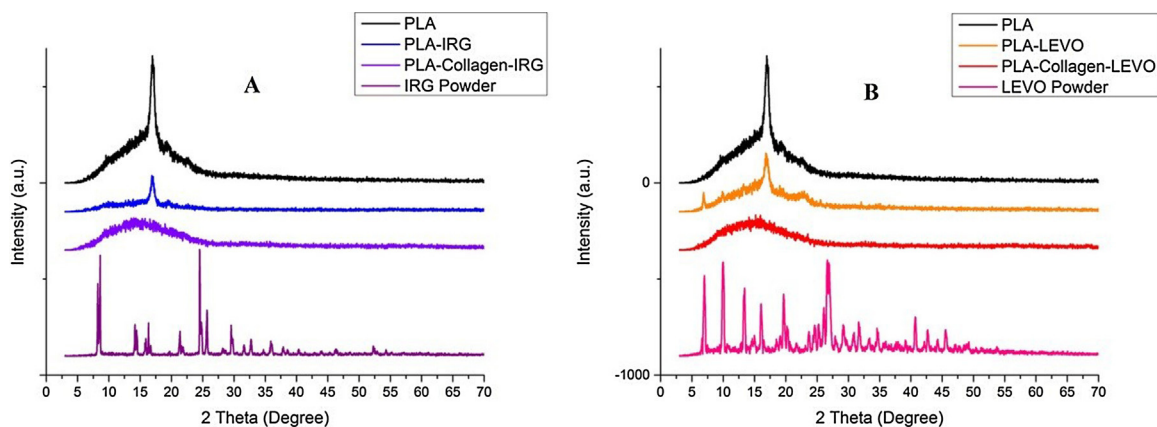**Fig. 5.** DSC Curves of (a) PLA-drug, (b) PLA-Collagen-drugs and (c) raw drugs Irgasan and Levofloxacin.

Fig. 6. XRPD Graphs of (a) PLA IRG Blends and (b) PLA LEVO Blends.

release behaviour over 192 h, with a final release of ∼40%. PLA-LEVO exhibited burst release behaviour, releasing ∼20% within the first 24 h of measurement. PLA-collagen-LEVO showed a significantly lower release percentage initially, however it appeared to exhibit sustained release behaviour, with a final cumulative release of 25%. The total drug content was determined by *Concentration × Volume of Medium × Dilution Factor/1000 (correction factor)*. Therefore, *% Drug Release = Amount of Drug/Theoretical Drug Amount × 100*.

Antibacterial measurements were taken at 24 h and 48 h (Fig. 9, 48 h only). The PLA-drug samples show a high efficacy to control the growth of both *E. coli* and *S. aureus*. In particular, PLA-LEVO (2.1 cm) had a higher average inhibition zone than PLA-IRG

(1.0 cm). PLA-collagen-IRG resisted both strains of bacteria in a similar manner to the PLA-IRG sample (average inhibition zone = 1.1 cm). Finally, the PLA-collagen-LEVO sample showed an average inhibition zone to *E. coli* of 1.0 cm; however white spores of bacteria were re-forming near the sample. This sample also had a smaller efficacy with inhibiting the growth of *S. aureus*, demonstrating an average inhibition zone of 0.4 cm.

3.6. ToF-SIMS

Imaging data showed a difference in the distribution of the APIs in the various strands. The compounds of interest are identified by unique characteristic ion peaks; PLA at m/z 71 ($[C_3H_3O_2]^-$) and m/z
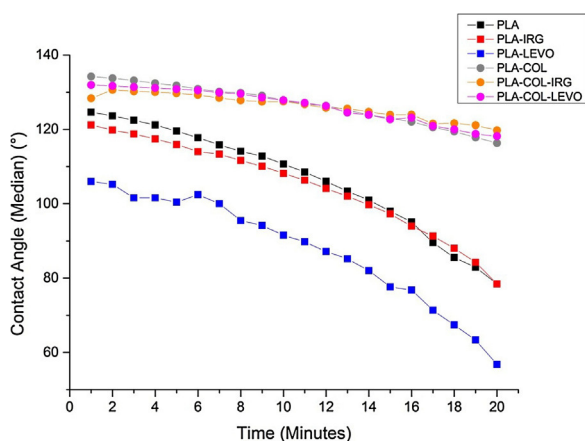
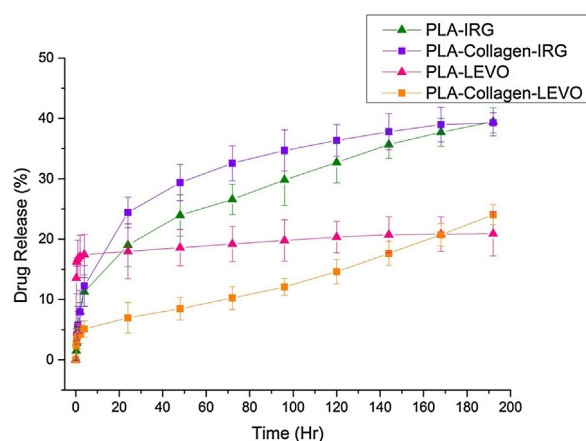Fig. 7. CAG Data for PLA-Drug and PLA-Collagen-Drug blends.

Fig. 8. Drug release profiles of PLA-drug and PLA-collagen-drug scaffolds.

89 ($[C_3H_5O_3]^-$), Levofloxacin at m/z 360 ($[C_{18}H_{19}FN_3O_4]^-$, $[M-H]^-$) and m/z 316 ($[C_{17}H_{19}FN_3O_2]^-$), and Irgasan at m/z 287 ($[C_{12}H_6{}^{35}Cl_3O_2]^-$ $[M-H]^-$), and isotopes m/z 289 ($[C_{12}H_6{}^{35}Cl_2{}^{37}ClO_2]^-$) and m/z 291 ($[C_{12}H_6{}^{35}Cl^{37}Cl_2O_2]^-$). The total ion images and the overlays of single ion images for the characteristic peaks of PLA, PLA-collagen and the two drugs are reported in Fig. 10. With regards to the PLA-IRG and PLA-LEVO electrospun scaffolds, by the ion images Irgasan appears to be homogeneously distributed throughout the sample, whilst the presence of Levofloxacin is concentrated in multiple small regions on the surface of the fibers. This confirms the data obtained with the AFM analysis and with the release study – (see: Results, Fibre Morphology and Results, Drug Efficacy).

The diagnostic peaks for both the APIs in the PLA-collagen-API samples present normalized intensities which are 2 to 3 times lower than the corresponding peaks in the PLA-API samples, making it difficult to comment on their distribution. The reduced signal could be caused by matrix effects, an artefact of ionization. Here, it is possible that the presence of collagen in the system suppressed the ionization of the APIs. Alternatively, it could suggest a lower concentration of the APIs present on the surface of the PLA-Collagen fibres compared to the PLA ones, and could be interpreted as a better embedding of the APIs into the strands.

4. Discussion

4.1. Fibre morphology

The differences in fibre form between PLA-drug and PLA-collagen-drug samples can be clearly seen in Figs. 2 and 3, where the addition of collagen has created smaller diameters of the fibres. This is due to the nature of collagen fibre formation, which usually form nanofibres of around 100 nm (Matthews et al., 2002). Although, the fibres created in this study are significantly bigger than other studies (e.g. average collagen fibres diameters = ~400 nm (Buttafoco et al., 2006)) this may be largely due to the blend of PLA and collagen – with PLA-drug solutions producing fibres with a diameter greater than 2 μm. Fibre formation may also be more effective with collagen, due to the HFP solvent; the low boiling point (58.2 °C) of this solvent allows for a quicker evaporation during the electrospinning process, which in turn means that the fibres are being deposited in a dry state. HFP is also a denaturing organic solvent, and therefore the interaction between solvent and collagen may cause change in the structure of the proteins (Guo et al., 2013). When compared to polycaprolactone fibres (as

conducted in our previous study) electrospun in similar conditions, the addition of levofloxacin increased the overall average fibre diameter (PCL = ~1.83 μm (Del Valle et al., 2011) PCL-LEVO = ~2.8 μm (Hall Barrientos et al., 2016)).

It was also observed that the addition of levofloxacin within both PLA and PLA-collagen blends resulted in a decreased average fibre diameter; this can be linked to the rheological behaviour of the solutions where levofloxacin increased the viscosity of the solution, which normally results in a change in fibre size (Song et al., 2012). There also appears to be evidence of levofloxacin appearing at the surface of the fibres (Fig. 4c), however this may be expected for this particular drug due to the high dispersive surface energy (see Results: Surface Analysis). If the drug has a high surface energy, this affects the viscosity of the solution, which in turn alters the surface tension.

The AFM images of the polymer-collagen blends revealed a helical pattern of collagen around the fibres – the fibrils of collagen exhibit a repeating, nano-banding pattern. Collagen naturally forms a coiled structure, and the underlying alpha chains within the collagen fibrils could be responsible for the repeating banding pattern observed (Barnes et al., 2007). This may be useful within a tissue engineering context, given that this repeat banding is thought to expose a binding site in the native collagen fibril that enhances cell adhesion and migration (Sell et al., 2009).

4.2. Solid state characterisation

The DSC data was vital in understanding any potential chemical interactions between the drug and polymer. In Fig. 5, the PLA-IRG plot, shows that there is no visible exothermic reaction (T_c) occurring after the initial glass transition phase, and also no indication of the T_m of the raw IRG drug at around 60 °C – this can interpreted as the IRG being fully integrated within the polymeric structure (Kayaci et al., 2013). The T_c values recorded were greater in the samples containing collagen which may be attributed to dehydration of the collagen (Bozec and Odlyha, 2011). This may be indicative of the collagen successfully embedding or interacting with the polymer. A reduction in the T_g at around 60 °C of the PLA-Collagen-LEVO can be observed, which again may indicate that there is no presence of free LEVO particle in this sample – this is perhaps why a sustained release behaviour is observed in Section 4.4 (drug efficacy).

The data presented by the DSC was effectively confirmed through the XRPD data (Fig. 6). The PLA-IRG sample can be seen to remain in a near semi-crystalline form (slight broad peak, followed by sharp crystalline PLA peak), with no IRG peaks. It can be
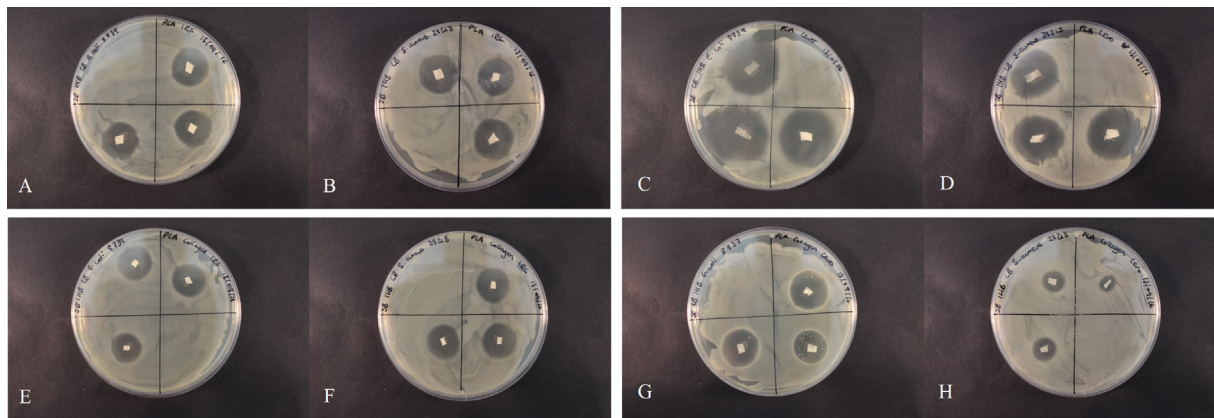
Fig. 9. Images of antibacterial growth after 48 h. (a) PLA-IRG against E. Coli, (b) PLA-IRG against S. Aureus, (c) PLA-LEVO against E. Coli, (d) PLA-LEVO against S. Aureus, (e) PLA-Collagen-IRG against E. Coli, (f) PLA-Collagen-IRG against S. Aureus, (g) PLA-Collagen-LEVO against E. Coli, and (h) PLA-Collagen-LEVO against S. Aureus.

concluded from this that the IRG is fully embedded within the polymeric network. Similarly, no IRG peaks were visible within the PLA-collagen-IRG graph; however, the broad peak does indicate that the material is in an amorphous form. The PLA-LEVO graph showed a peak, indicating that the drug is still in crystalline form and is not incorporated uniformly into the polymeric network. A similar amorphous peak was observed in the PLA-collagen-LEVO peak, which may indicate a better encapsulation of drug.

4.3. Surface analysis

Understanding the surface energy of the drug molecules was an important part of this study, since it has successfully helped to understand the reasons behind particular behaviour relating to fibre morphology and overall drug encapsulation. The surface energy analysis of the two drugs indicated a higher dispersive surface energy for levofloxacin compared with irgasan. Given that IRG and LEVO are both in a crystalline form, and that polylactic acid is naturally semi-crystalline, there may be an increased possibility of the two drugs integrating into the polymeric matrix. The two drugs may require a higher energy in order to disperse properly within the PLA polymeric structure. With irgasan having a lower dispersive surface energy and a hydrophobic nature, there may be a reduced energy requirement for this drug to properly disperse within a solvent solution. If levofloxacin has a higher dispersive surface energy, then the transfer of energy between LEVO and solvent will be insufficient to overcome the drug–drug attractions. Therefore, not all the levofloxacin molecules in solution will be surrounded by solvent molecules and dispersed fully into solution (Shah et al., 2017). At equilibrium, hydrophobic molecules preferentially partition into the organic phase, typically due to a high log P value (Vorng et al., 2016) – the log P of levofloxacin is 1.27 (Anon., 2008a) and the log P of Irgasan is 4.76 (Anon., 2008b). Based on the positive values on the log P, both drugs are hydrophobic and Irgasan is more hydrophobic than LEVO. With both drugs and PLA exhibiting a hydrophobic nature, this suggests that hydrophobic interactions might occur between the materials. If the hydrophobic interactions are a dominant, this should be more advantageous in increasing encapsulation efficiency (Jeyanthi et al., 1997).

The change in contract angle may reflect the encapsulation of both drugs within the polymer matrix. It can be clearly seen in Fig. 7 that the contact angle was lowest for the PLA-LEVO sample. This can be attributed to the lower hydrophobic nature of levofloxacin, the high dispersive surface energy and the probability of the drug on the surface of the fibres (see Results: Fibre

Morphology, AFM). With the PLA-collagen-drug samples, the contact angles are greater, implying that the samples are more hydrophobic. These results differ from the contact angle measurements in other studies, in particular collagen is found to have previously increased the hydrophilicity of PLA samples (Ahmed et al., 2015). It may be the case that the collagen fibrils have interacted within the polylactic acid based nanofibre. This strong hydrophobic connection may be linked to the better integration of both irgasan and levofloxacin.

4.4. Drug efficacy

The release profiles of both irgasan and levofloxacin are similar to the results in a previous study using *polycaprolactone* (Hall Barrientos et al., 2016). However, the final cumulative release percentages with *Polylactic acid* appear to be lower (Final PCL scaffolds drug release ∼50%, PLA scaffolds ∼20% to 40%). This may suggest a poorer drug encapsulation with PLA, which may be due to the fact that PLA is more hydrophilic than PCL (Patrício et al., 2013). The hydrophobic interactions between PLA and IRG may potentially be the cause of the sustained release behaviour *in vitro*, and the lower hydrophobic nature of LEVO may be an even further reduction in a strong polymer-drug interaction. As mentioned in the surface analysis section, the higher dispersive surface energy may cause this weak interaction between PLA and LEVO; AFM images in Fig. 4 indicating the possible presence of drug at the surface of the fibres. This presence of drug at the surface would result in a rapid uptake of water, and therefore be the reason behind the burst release behaviour observed *in vitro*. The addition of type I collagen to the polymer-drug samples resulted in a difference in release behaviour with LEVO – this drug released in a sustained release time profile, implying that collagen may be directly affecting the release of the drug. Literature evidence suggests that the hydrophilic, carboxyl functional groups in the polymer could be interacting with basic functions expressed by the collagen (Cheng and Teoh, 2004) which in turn results in a change in the hydrophobicity of the fibre, which may result in the sustained release time profile for the levofloxacin with the PLA-collagen sample.

The antibacterial studies were consistent with the drug release profiles, and indicated that the formulations were effective in inhibiting the growth of *E. coli* and *S. aureus*. The larger zones of inhibition can be seen in the PLA-LEVO sample, which exhibits burst release behaviour. The smaller inhibition zones for PLA-IRG and PLA-collagen-IRG were indicative of the sustained release profiles. The sustained release profile of PLA-collagen-LEVO was
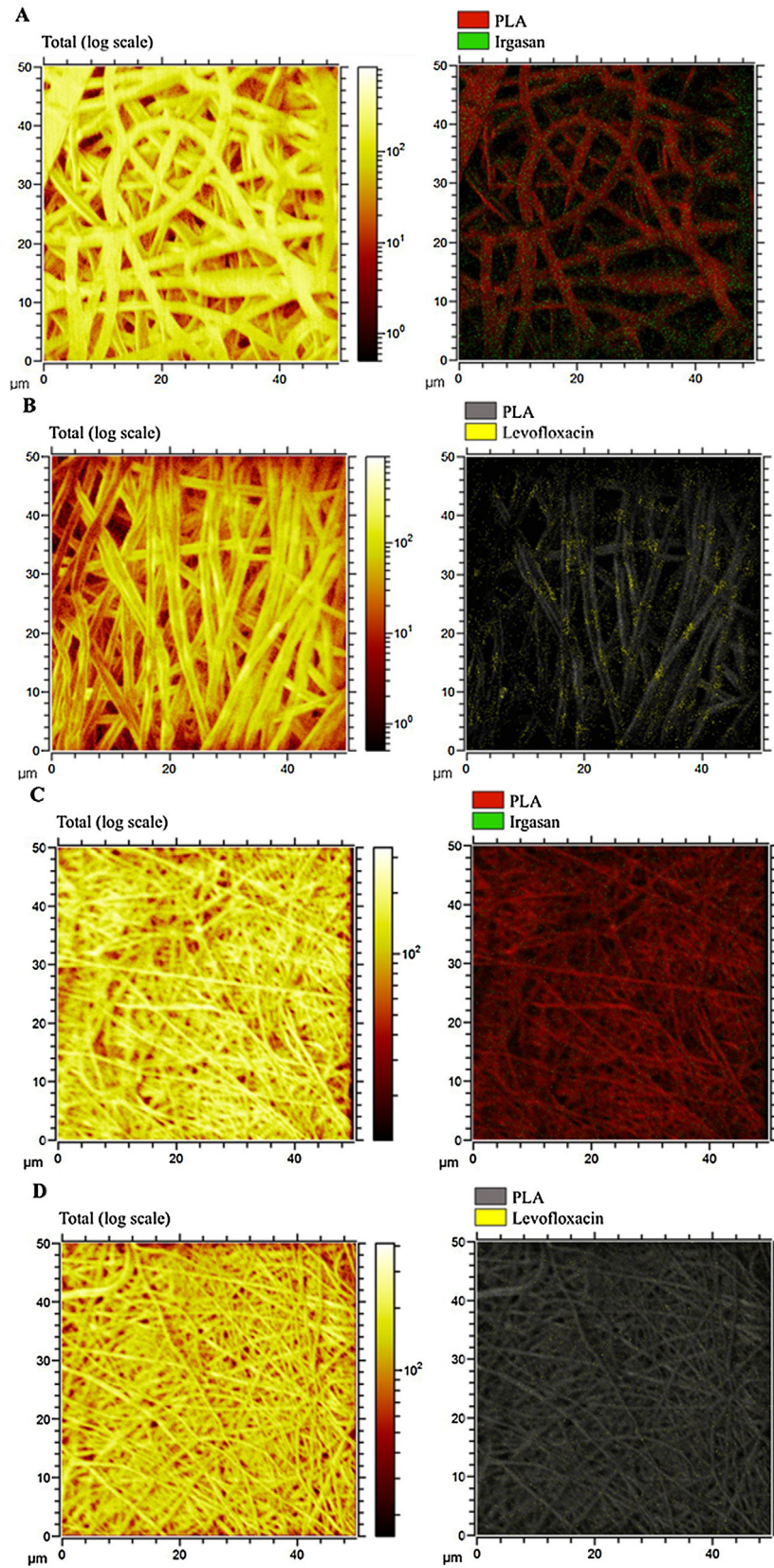
Fig. 10. ToF-SIMS data of (a) PLA-IRG, (b) PLA-LEVO, (c) PLA-Collagen-IRG, and (d) PLA-Collagen-LEVO.

also confirmed, given that there were small areas of bacterial growth – this can be attributed to the low cumulative release percentage at 48 h of the study by which time <10% of the drug had been released).

4.5. ToF-SIMS

The visualisation of the distribution of the APIs on the sample surface contributed to gain a better understanding about the degree of drug encapsulation and in general about the interactions between the drugs and the fibres. This result concurs with the suggested explanation with regards to the release behaviour and is consistent with the results from the other techniques described in this paper.

5. Conclusion

It can be seen that the inclusion of type I collagen significantly altered various characteristics of electrospun polymer-drug scaffolds. The addition of collagen caused an overall decrease in fibre morphology and average fibre diameter across both sets of drugs, irgasan and levofloxacin, with nanofibers forming in the PLA-collagen-LEVO samples. AFM images revealed collagen fibril banding on the surface of the fibres which suggest there is an interaction between the polymer-drug and collagen. There were also changes in the solid-state characteristics of the samples, given that the DSC results indicate an increase in amorphousness of the polymer-drug-collagen samples, and this was confirmed through typically broad peaks in the XRPD results. Most interestingly, the surface energies of the scaffolds were modified with an increase in the hydrophobicity of the polymer-collagen-drug noted. In particular, the PLA-collagen-LEVO sample showed a high deal of hydrophobicity, which was unusual given the low hydrophobic nature of LEVO – this could potentially be attributed to the strong hydrophobic interactions between the PLA and the hydrophobic banding in collagen fibrils, resulting in better encapsulation of the drug. Finally, the drug release profiles of the samples appear to change due to the inclusion of collagen, most significantly demonstrating the shift of the burst release behaviour in PLA-LEVO to sustained release behaviour within PLA-collagen-LEVO samples. This study is important in demonstrating that the modification of electrospun scaffolds can be achieved by incorporating natural polymers, such as collagen – and this modification may be useful in the compatibility and utilisation of tissue engineered structures within the human body.

References

Ahmed, M., et al., 2015. A combinatorial approach towards the design of nanofibrous scaffolds for chondrogenesis. Sci. Rep. 5, 1–12.

Anon, 2008a. Levofloxacin. Tuberculosis 88, 119–121.

Anon, 2008b. Nomination Profile Triclosan Supporting Information for Toxicological Evaluation by the National Toxicology Program. U.S. Food Drug Adm..

Athanasiou, K.A., Niederauer, G.G., Agrawal, C.M., 1996. Sterilization, toxicity, biocompatibility and clinical applications of polylactic acid/polyglycolic acid copolymers. Biomaterials 17, 93–102.

Barnes, C.P., Pemble, C.W., Brand, D.D., Simpson, D.G., Bowlin, G.L., 2007. Cross-linking electrospun type II collagen tissue engineering scaffolds with carbodiimide in ethanol. Tissue Eng. 13, 1593–1605.

Bozec, L., Odlyha, M., 2011. Thermal denaturation studies of collagen by microthermal analysis and atomic force microscopy. Biophys. J. 101, 228–236.

Buttafoco, L., et al., 2006. Electrospinning of collagen and elastin for tissue engineering applications. Biomaterials 27, 724–734.

Cheng, Z., Teoh, S.H., 2004. Surface modification of ultra thin poly (epsilon-caprolactone) films using acrylic acid and collagen. Biomaterials 25, 1991–2001.

Del Valle, L.J., et al., 2011. Electrospinning of polylactide and polycaprolactone mixtures for preparation of materials with tunable drug release properties. J. Polym. Res. 18, 1903–1917.

Gamble, J.F., et al., 2012. Surface energy analysis as a tool to probe the surface energy characteristics of micronized materials – a comparison with inverse gas chromatography. Int. J. Pharm. 422, 238–244.

Guo, C., Zhou, L., Lv, J., 2013. Effects of expandable graphite and modified ammonium polyphosphate on the flame-retardant and mechanical properties of wood flour-polypropylene composites. Polym. Polym. Compos. 21, 449–456.

Hall Barrientos, I.J., et al., 2016. Fabrication and characterisation of drug-loaded electrospun polymeric nanofibers for controlled release in hernia repair. Int. J. Pharm. 517, 329–337.

He, T., et al., 2015. Electrospinning polyvinylidene fluoride fibrous membranes containing anti-bacterial drugs used as wound dressing. Colloids Surf. B Biointerfaces 130, 278–286.

He, M., Jiang, H., Wang, R., Xie, Y., Zhao, C., 2016. Fabrication of metronidazole loaded poly (ε-caprolactone)/zein core/shell nanofiber membranes via coaxial electrospinning for guided tissue regeneration. J. Colloid Interface Sci. 490, 270–278.

Hu, M.S., et al., 2014. Tissue engineering and regenerative repair in wound healing. Ann. Biomed. Eng. 42, 1494–1507.

Jeyanthi, R., Mehta, R.C., Thanoo, B.C., Deluca, P.P., 1997. Effect of processing parameters on the properties of peptide-containing PLGA microspheres. J. Microencapsul. 14, 163–174.

Jiang, Q., Reddy, N., Zhang, S., Roscioli, N., Yang, Y., 2013. Water-stable electrospun collagen fibers from a non-toxic solvent and crosslinking system. J. Biomed. Mater. Res. – Part A 101 A, 1237–1247.

Kayaci, F., Umu, O.C.O., Tekinay, T., Uyar, T., 2013. Antibacterial electrospun poly (lactic acid) (PLA) nano fibrous webs incorporating Triclosan/Cyclodextrin inclusion complexes. J. Agric. Food Chem. 61, 3901–3908.

Kimura, H., Ogura, Y., 2001. Biodegradable polymers for ocular drug delivery. Ophthalmologica 4678601, 143–155.

Koh, T.J., DiPietro, L.A., 2011. Inflammation and wound healing: the role of the macrophage. Expert Rev. Mol. Med. 13, 1–14.

Lamprou, D.A., et al., 2010. Self-assembled structures of alkanethiols on gold-coated cantilever tips and substrates for atomic force microscopy: molecular organisation and conditions for reproducible deposition. Appl. Surf. Sci. 256, 1961–1968.

Lamprou, D.A., Venkatpurwar, V., Kumar, M.N.V.R., 2013. Atomic force microscopy images label-free, drug encapsulated nanoparticles in vivo and detects difference in tissue mechanical properties of treated and untreated: a tip for nanotoxicology. PLoS One 8, 8–12.

Mano, J.F., et al., 2007. Natural origin biodegradable systems in tissue engineering and regenerative medicine: present status and some moving trends. J. R. Soc. Interface 4, 999–1030.

Matthews, J.A., Wnek, G.E., Simpson, D.G., Bowlin, G.L., 2002. Electrospinning of collagen nanofibers. Biomacromolecules 3, 232–238.

McManus, M.C., Boland, E.D., Simpson, D.G., Barnes, C.P., Bowlin, G.L., 2006. Electrospun fibrinogen: feasibility as a tissue engineering scaffold in a rat cell culture model. J. Biomed. Mater. Res. – Part A 81A, 299–309.

Nair, P., Schug, J., 2004. Observations on healing of human tooth extraction sockets implanted with bioabsorbable polylactic-polyglycolic acids (PLGA) copolymer root replicas: a clinical, radiographic, and histologic follow-up report of 8 cases. Oral Surg. Oral Med. Oral Pathol. Oral Radiol. Endod. 97, 559–569.

Patrício, T., Domingos, M., Gloria, A., Bártolo, P., 2013. Characterisation of PCL and PCL/PLA scaffolds for tissue engineering. Procedia CIRP 5, 110–114.

Powell, H.M., Boyce, S.T., 2009. Engineered human skin fabricated using electrospun Collagen–PCL blends: morphogenesis and mechanical properties. Tissue Eng. Part A 15 doi:http://dx.doi.org/10.1089/Ten.Tea.2008.0473.

Rafqah, S., Wong-Wah-Chung, P., Nelieu, S., Einhorn, J., Sarakha, M., 2006. Phototransformation of triclosan in the presence of TiO2 in aqueous suspension: mechanistic approach. Appl. Catal. B Environ. 66, 119–125.

Ramot, Y., Haim-Zada, M., Domb, A.J., Nyska, A., 2016. Biocompatibility and safety of PLA and its copolymers. Adv. Drug Deliv. Rev. 107, 153–162.

Sell, S.A., McClure, M.J., Garg, K., Wolfe, P.S., Bowlin, G.L., 2009. Electrospinning of collagen/biopolymers for regenerative medicine and cardiovascular tissue engineering. Adv. Drug Deliv. Rev. 61, 1007–1019.

Shah, N., Sandhu, H., Choi, D.S., Chokshi, H., Malick, A.W., 2017. Fundamentals of Amorphous Systems: Thermodynamic Aspects. Amorphous Solid Dispersions. Springer US, 2014 doi:http://dx.doi.org/10.1007/978-1-4939-1598-9.

Shahwal, V.K., Dubey, B.K., Bhoumick, M., 2013. Preformulation study of levofloxacin. Int. J. Adv. Pharm. 1, 1–8.

Solomkin, J.S., et al., 2010. Diagnosis and management of complicated intra-abdominal infection in adults and children: guidelines by the Surgical Infection Society and the Infectious Diseases Society of America. Clin. Infect. Dis. 50, 133–164.

Song, B., Wu, C., Chang, J., 2012. Dual drug release from electrospun poly(lactic-co-glycolic acid)/mesoporous silica nanoparticles composite mats with distinct release profiles. Acta Biomater. 8, 1901–1907.

Tan, A.R., et al., 2008. Electrospinning of photocrosslinked and degradable fibrous scaffolds. J. Biomed. Mater. Res. − Part A 87, 1034–1043.

Tillman, B.W., et al., 2009. The in vivo stability of electrospun polycaprolactone-collagen scaffolds in vascular reconstruction. Biomaterials 30, 583–588.

Toncheva, A., Paneva, D., Manolova, N., Rashkov, I., 2011. Electrospun poly(L-lactide) membranes containing a single drug or multiple drug system for antimicrobial wound dressings. Macromol. Res 19, 1310–1319.

van Winterswijk, P.J., Nout, E., 2007. Tissue engineering and wound healing: an overview of the past, present, and future. Wounds 19.

Venugopal, J., Zhang, Y.Z., Ramakrishna, S., 2005. Fabrication of modified and functionalized polycaprolactone nanofibre scaffolds for vascular tissue engineering. Nanotechnology 16, 2138–2142.

Vorng, J.-L., et al., 2016. Semi-empirical rules to determine drug sensitivity and ionization efficiency in SIMS using a model tissue sample. Anal. Chem. 88, 11028–11036.